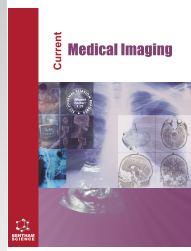




CrossMark

# Current Medical Imaging

Content list available at: <https://benthamscience.com/journals/cmir>

## RESEARCH ARTICLE

### A Lightweight Super-resolution Network with Skip-connections

Xuzhou Wu<sup>1</sup>, Pingping Dai<sup>1</sup>, Shi Lu<sup>1</sup>, Zhendong Luo<sup>2</sup>, Jirang Sun<sup>3</sup> and Kehong Yuan<sup>1,\*</sup><sup>1</sup>*Graduate School at Shenzhen, Tsinghua University, Shenzhen, China*<sup>2</sup>*Department of Radiology, The University of Hong Kong - Shenzhen Hospital, Shenzhen, China*<sup>3</sup>*Sanbo Brain Hospital, Capital Medical University, Beijing, China*
**Abstract:**
**Introduction:**

In some hospitals in remote areas, due to the lack of MRI scanners with high magnetic field intensity, only low-resolution MRI images can be obtained, hindering doctors from making correct diagnoses. In our study, high-resolution images can be obtained through low-resolution MRI images. Moreover, as our algorithm is a lightweight algorithm with a small number of parameters, it can be carried out in remote areas under the condition of the lack of computing resources. Moreover, our algorithm is of great clinical significance in providing references for doctors' diagnoses and treatment in remote areas.

**Methods:**

We compared different super-resolution algorithms to obtain high-resolution MRI images, including SRGAN, SPSR, and LESRCNN. A global skip connection was applied to the original network of LESRCNN to use global semantic information to get better performance.

**Results:**

Experiments reported that our network improved SSIM by 0.8% and also achieved an obvious increase in PSNR, PI, and LPIPS compared to LESRCNN in our dataset. Similar to LESRCNN, our network has a very short running time, the small number of parameters, low time complexity, and low space complexity while ensuring high performance compared to SRGAN and SPSR. Five MRI doctors were invited for a subjective evaluation of our algorithm. All agreed on significant improvements and that our algorithm could be used clinically in remote areas and has great value.

**Conclusion:**

The experimental results demonstrated the performance of our algorithm in super-resolution MRI image reconstruction. It allows us to obtain high-resolution images in the absence of high-field intensity MRI scanners, which has great clinical significance. The short running time, a small number of parameters, low time complexity, and low space complexity ensure that our network can be used in grassroots hospitals in remote areas that lack computing resources. We can reconstruct high-resolution MRI images in a short time, thus saving time for patients. Our algorithm is biased towards clinical and practical applications, and doctors have affirmed the clinical value of our algorithm.

**Keywords:** Super-resolution, lightweight, MRI images, Doctors diagnosis, Evaluation algorithm.

**Article History**

Received: December 16, 2022

Revised: March 13, 2023

Accepted: March 17, 2023

## 1. INTRODUCTION

### 1.1. Background

The structure of the brain is relatively complex. It contains complex tissues, such as the cerebral cortex, grey matter, white matter, and cerebrospinal. White matter is covered with grey matter, while grey matter forms groove back easily. Compared

to other medical imaging techniques, Magnetic Resonance Imaging (MRI) images have higher contrast and spatial resolution at a smaller cost of ionizing radiation and non-invasive damage to the human body. Therefore, MRI is widely used in brain disease analysis. The image intensity distribution of different brain tissue MRI images is always uneven and overlapping; thus, the analysis of brain MRI images is of great significance for medical diagnosis.

\* Address correspondence to this author at the Graduate School at Shenzhen, Tsinghua University, Shenzhen, China; E-mail: [yuankh@sz.tsinghua.edu.cn](mailto:yuankh@sz.tsinghua.edu.cn)

In recent years, medical imaging techniques, such as MRI, have been widely used in medical diagnosis. These techniques allow doctors to observe the inner change in organs so that doctors can diagnose accurately, develop treatment plans, and test the effectiveness of treatment. Many lesions induce the deformation of tissues or organs or are induced by the deformation of tissues or organs. For instance, atrophy of the cerebral cortex causes Alzheimer's disease, and tumor deterioration can cause bulges on the surface of the organ. Doctors diagnose by measuring whether an organ is mutated by comparing changes in its shape and analyzing morphological changes around the tumor to determine the location of the tumor. Such diagnoses and multimodal fusion need medical image enhancement techniques, such as image super-resolution and registration, as preprocessing and measurement.

In order to improve the quality of MRI images to assist in diagnosis, deep learning methods have been gradually applied in MRI image processing in recent years.

With the rapid development of MRI technology, image resolution has continued to increase. However, in clinical practical applications, due to factors, such as equipment price and technician experience, the resolution of the MRI dataset has a certain difference. In primary hospitals in remote areas, there are problems, such as backward MRI equipment, low magnetic field intensity, and low imaging resolution, which are not conducive to diagnosis. In this study, the super-resolution algorithm was used to enhance MRI images, and the low-resolution images were used to generate high-resolution images. In addition, due to the lack of computing resources in primary hospitals, this study adopts the algorithm with a low reference quantity. Most of the current super-resolution algorithms are aimed at natural images. However, MRI images have many differences from natural images; in order to improve the performance of super-resolution algorithms on MRI images, we evaluated several current super-resolution algorithms with our collected MRI dataset on multiple evaluation metrics. According to the characteristics of medical image data, we proposed Enhanced-LESRCNN with global skip-connection, which makes full use of hierarchical features of low-resolution images. In this study, the super-resolution algorithm was used to enhance the MRI image to generate high-resolution images with equipment of low magnetic field intensity. In addition, due to the lack of computing resources in primary hospitals, this study adopts a lightweight algorithm to solve the problem of inadequate medical resources in primary hospitals.

## 1.2. Related work

MR imaging plays an important role in assisting doctors in diagnosis and quantitative analysis. With the progress in the production techniques of MRI inspection equipment, the magnetic field strength type of MRI has changed from only 0.5T to 1.0T, 1.5T, 3.0T and other different levels. In general, the higher the magnetic field intensity of the MRI, the higher the image resolution and image quality of the imaging. MRI datasets are diverse in image resolution and image quality. When performing registration and joint analysis between different datasets of MRI, due to the different device models

used in different datasets and the setting of magnetic field strength, it is common to encounter different resolutions between different datasets. To improve the consistency of multiple datasets, the task of super-resolution generation of low-resolution MRI images has become significant. At the same time, in the application scenarios of auxiliary medical diagnosis and quantitative analysis of medical images, high-resolution MRI images can provide more detailed anatomical information than low-resolution images. The acquisition of high-resolution MRI images often requires more advanced inspection equipment with higher magnetic field strength, which is hard to acquire in ordinary hospitals. Therefore, the use of image super-resolution technology to generate high-resolution MRI images using low-resolution MRI images has great significance for the lack of high-precision medical devices.

Image super-resolution is one of the vital image processing methods in computer vision. Significant progress has been made in this area in the past few decades. We introduced the evolution of super-resolution algorithms in two parts, classical methods of super-resolution and deep-learning-based methods of super-resolution.

The classical image super-resolution methods mainly include methods based on prediction, interpolation, and sparse representation methods. The early image restoration methods are based on prediction. The first method [1] was a Fourier method of filtering digital data called Lanczos filtering using the "sigma factor," which reduces the amplitude of the Gibbs oscillation. The methods of the interpolation class consist of bilinear interpolation (bilinear), bicubic interpolation (bicubic), etc. Methods based on sparse representation appeared around 2008. Yang [2] and others proposed a series of sparse representation methods and applied them in performing various tasks. Gao [3] applied the locally linear embedding method in manifold learning to image super-resolution in 2012, and Gu [4] used a convolutional sparse coding method for image super-resolution. Super-resolution generation is an ill-posed problem because there can be several high-resolution images corresponding to the same low-resolution image, making the super-resolution a conversion of many-to-one process. Simple image interpolation will lead to the blurring of features and edges within the sample image. As for the feature extraction of MRI images, some traditional methods have achieved good results, especially the random walk algorithm. Dakua achieved good results [5], and results were further improved in subsequent work [6]. It is of vital importance for the super-resolution method to learn high-order texture features of the low-resolution images, in which deep-learning methods are adapted.

With the development of deep learning methods in computer vision, deep learning networks are widely used in various computer vision tasks, and super-resolution algorithms based on deep learning show superior performance. SRCNN proposed by Dong *et al.* [7] is the pioneering work of deep learning application in image super-resolution generation, which uses double cubic interpolation (bicubic) to enlarge the low-resolution image to the corresponding size and then use a three-layer convolutional neural network to fit a nonlinear map

towards output super-resolution image. Kim [8] applied the idea of the residual network (ResNet) to image super-resolution, using deep networks to learn residuals between high-resolution images and low-resolution images. Johnson *et al.* [9] employed a perceptual loss function to make the resulting high-resolution images visually more reliable. Ledig *et al.* [10] proposed that SRGAN employed the generative adversarial network to solve the problem of super-resolution, using perceptual loss, generative loss, and adversarial loss to improve the realism of the generated pictures [10]. More GAN-based methods were proposed later, such as ESRGAN [11] and SPSR [12], which were improved by proposing new network structures or supervising information.

In recent years, more super-resolution methods have been modified to have better performance in applications for medical images. Methods of super-resolution can also be categorized into single-image super-resolution (SISR) and multiple-image approaches. Although the proportion of 3D medical images is increasing, medical 3D images are generally obtained by stacking their 2D slice imaging. Therefore, Single Image Super-Resolution technologies are still mainly used to process medical images. Compared with natural images, medical images have more low-level texture detail information, and most of the focus is characterized by small-scale targets, so there are many specific designs in the network structure targeting medical images. Caballero *et al.* [13] applied the super-resolution method of sparse representation and dictionary learning to the super-resolution generation of cardiac MRI images in 2013. In 2017, GAO *et al.* [14] added secondary feature extraction and pooling layers based on SRCNN for the super-resolution reconstruction of CT images. In 2018, Liu *et al.* [15] proposed that SR-DCNN achieved good results in super-resolution of medical images, such as the heart and spine. Ren *et al.* [16] proposed a medical image super-resolution algorithm based on a deep residual network in 2019, using a multi-scale model applied to medical images of different scales. Bing *et al.* [17] applied GAN to medical image super-resolution and proposed a new fusion function. In 2020, Chen *et al.* improved the integration of SRGAN and DenseNet features, proposed a deep convolutional neural network, and

introduced a feedback mechanism to enhance the reconstruction performance of medical images.

As for brain image super-resolution, the brain MR images have a relatively fixed structure (images of a single organ) and contain less contextual information compared to the natural image datasets, such as DIV2K [18], commonly used for super-resolution methods evaluation. This feature of every level of the neural network is valuable in brain image processing. There have been a few studies on super-resolution reconstructions of brain MRI images. Zheng [19] established a relationship model of gradient value between different contrast images to obtain high-resolution images. De Leeuw den Bouter [20] presented a deep learning approach based on dense connections to achieve super-resolution reconstruction. Aiming to investigate the super-resolution methods applied in brain MR images, we first evaluated three advanced deep-learning-based image super-resolution methods which were proposed lately. We verified the effectiveness of these methods on a brain MRI dataset, containing images of heterogeneous magnet field strength collected from several hospitals. We analyzed their pros and cons and proposed enhanced LESRCNN with global skip-connection, which uses all hierarchical features of the information extraction network and achieves higher performance on the MRI dataset.

## 2. METHODS

### 2.1. Definition of Image Super-resolution

Image super-resolution (SR) is one of the important research directions in computer vision. It refers to the technology of improving image resolution through software methods without improving imaging hardware. Image super-resolution is valuable in video security surveillance, satellite remote sensing imaging, and medical imaging. A large number of signal processing methods and today's deep learning methods are heavily applied in this field.

Specifically, the purpose of image super-resolution is to recover the corresponding high-resolution image (HR) from a low-resolution image (LR). Low-resolution images are generally degraded from high-resolution images.

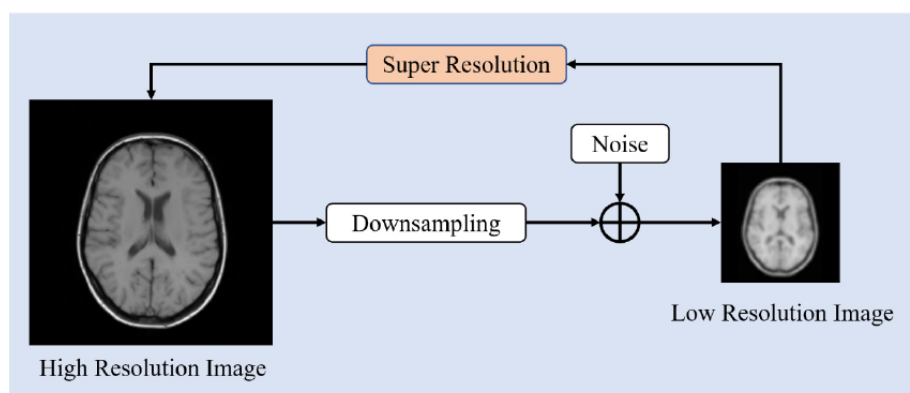


**Fig. (1).** The process of image super-resolution.

$$I_x = D(I_y; \delta) \quad (1)$$

Where,  $I_x$  is a low-resolution image,  $I_y$  is a raw high-resolution image,  $D$  is a degraded function, and  $\delta$  is degradation-dependent parameters, such as noise type or scaling parameters. The goal of super-resolution generation is to generate the corresponding  $\hat{I}_y$  with help of  $I_x$  to restore the high-resolution image  $I_y$ :

$$\hat{I}_y = F(I_x; \theta) \quad (2)$$

As shown in Fig. (1), the goal of the image super-resolution model can be understood as training to generate model parameters:

$$\hat{\theta} = \operatorname{argmin}_{\theta} L(\hat{I}_y, I_y) + \lambda \phi(\theta) \quad (3)$$

Where  $L$  is the loss function, and  $\phi$  is the regularization term for the model parameters.

## 2.2. Enhanced LESRCNN with Global Skip-Connections

### 2.2.1. Skip Connections for Medical Images Processing

The medical image structure is relatively fixed, and the semantic information of the image is relatively simple; thus, the semantic information of each layer of feature space has meaning in training. In the LESRCNN, the local features of the first layer and the global features of the tail layer are integrated for training to solve the problem of long-term dependence on the network. Referring to the skip connection idea from UNet, the original network information extraction and enhancement (IEEB) module, every feature of the layer in the information extraction block is fed into the tail layer network together in the form of concatenation and uses a convolutional layer of  $1*1$  so that the features of all layers are weighted and fused so that the network maximizes the utilization of the feature space of each layer. We do not use a pooling layer or convolution layer with a stride greater than 1 to downsample in the feature extraction module IEEB, so the resolution of each layer is the same, and there is no size constraint during concatenation. At the same time, according to experiments conducted by Zhang

[21], the performance of the super-resolution model on the perceptual similarity index has a strong relationship with its distance to the ground truth in the high-dimensional feature space, and the performance of the perceptual similarity index can also be improved by making full use of the feature output of each layer of the network.

### 2.2.2. LESRCNN with Global Skip-Connections

In this study, the above global skip connection idea is applied to the original network of LESRCNN [22], and a global skip connection network is built, referred to as ELESRCNN, as shown in Fig. (2).

The input to the network is degraded LR (low-resolution) picture data with three channels of RGB. The network consists of three modules: the Information Extraction and Enhancement Block (IEEB), the Reconstruction Module (RB), and the Information refinement Block (IRB). In the Information Extraction and Enhancement Module, the (IEEB) module consists of a total of 17 sequentially connected  $3*3$  convolutional layers and  $1*1$  convolutional layers stacked, each of which is connected to a layer of ReLU activation functions. The size of the first layer parameter is  $3*3*3*64$ , of which 3,  $3*3$ , and 64 are the number of input channels, the size of the convolutional kernel, and the number of output channels. The next odd (1, 3, 5,...,17) layer network layer is a  $3*3$  convolutional network layer + ReLU activation layer with a parameter size of  $64*3*3*64$ , where 64,  $3*3$ , 64 are the number of input channels, convolutional kernel size, and the number of output channels, respectively. Similarly, the even (2, 4, 6,...,16) layer is a  $1*1$  convolutional layer of  $64*1*1*64$  followed by ReLU activation layer. Referring to ResNet's residual network module, the output of each  $3*3$  network layer will be fused into the next  $3*3$  convolutional network layer through skip connection into the ReLU activation layer.  $C_3$  and  $C_1$  represent the convolutional layers with size of  $3*3$  and  $1*1$ .  $R()$  represents the ReLU activation function,  $O_c^j$  represents the output of the  $j$ -layer convolutional network,  $O^i$  represents the output of the Layer i. The information extraction enhancement block for the network can be represented as:

$$O_c^j = \begin{cases} C_3(O^{j-1}) & j \text{ is odd} \\ C_1(O^{j-1}) & j \text{ is even} \end{cases} \quad (4)$$

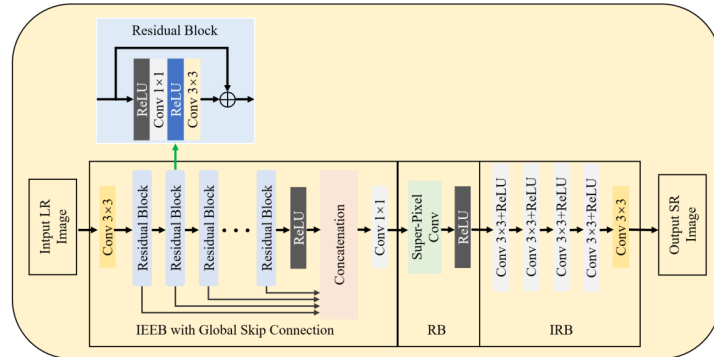


**Fig. (2).** Structure of LESRCNN.

$$O^i = \begin{cases} R(O_c^i + \sum_{i=1}^{i-2} O_c^i) & i \text{ is odd} \\ R(O_c^i) & i \text{ is even} \end{cases} \quad (5)$$

We use each of the features extracted by the previous module and each  $3*3$ +ReLU convolutional layer for feature fusion and then enter a  $1*1$  convolutional layer adaptive weighting to select the input features. Then in the Reconstruction Block, we use a subpixel convolutional layer from the adaptive selection of a scale factor of  $2*2$ ,  $3*3$ , or  $4*4$ . Among them, the scale factors of  $2*2$  and  $3*3$  were realized by a  $2*2$  and  $3*3$  convolutional layer combined with a shuffle\*2 layer, respectively, while the scaling factor of  $4*4$  was realized by two  $2*2$  equal-size convolutional layers combined with shuffle\*2 layers.

Using  $O_{RB}$  to present the output of the reconstruction module,  $O_n$  to represent the output of the nth layer,  $S()$  to represent the output of sub-pixel convolution, the output of the module can be expressed as:

$$O_{RB} = R(S(O_1) + S(O_3) + S(O_5) + \dots + S(O_{17})) \quad (6)$$

After obtaining the large-size feature map through the scaling factor, continue to enter an information purification block consisting of four  $3*3$  Conv+ReLU layer and one  $3*3$  Conv layer in series to further learn the information of high-dimensional features. The final output super-resolution image is represented in  $O_{SR}$ :

$$O_{SR} = C_3(R\left(C_3\left(R\left(C_3\left(R\left(C_3\left(R\left(C_3\left(O_{RB}\right)\right)\right)\right)\right)\right)\right)) \quad (7)$$

### 3. RESULTS AND DISCUSSION

A total of 29315 MR images with different magnetic field settings were collected, including 13820 0.5T images, 15495 1.5T images, and 3.0T images, while 0.5T, 1.5T, and 3.0T represented the magnetic field strength setting. All images were  $256*256$ , but a higher magnetic field setting indicated a higher resolution. The datasets of different resolutions were divided into training sets and validation sets, and the specific number of images is shown in Table 1.

**Table 1. Magnetic field strength of collected dataset.**

0.5T	0.5T	1.5T	1.5T	Total
Train	Test	Train	Test	
11870	1950	13160	2335	29315

We downsampled the collected training set pictures based on the principle of magnetic resonance imaging to obtain a low-resolution  $64*64$  input image and used the three super-resolution frameworks built to perform super-resolution reconstruction training.

We employed the method of transfer learning in the training process of the super-resolution network using the natural image dataset ImageNet for the super-resolution task to

obtain the pre-trained weight values and used the MRI data collected by ourselves based on the pre-training weights to obtain the final weight parameters by fine-tuning. The specific training steps were, first, through the downsampling method, the training set data was selected from the DIV2K dataset, and the low-resolution image was downsampled; then, the generated low-resolution image was trained by using the super-resolution framework built to generate the original resolution image for model training, and the same parameters were used to continue training for 10 rounds, which could enable the network to fine-tune the convolutional kernel weight value for the new low-resolution input, and then, we finally obtained the pre-trained weights of the super-resolution network.

Subsequently, the collected MRI image data was used, the pre-training weights obtained above were used as the initialization parameters, and the super-resolution network continued to be trained and fine-tuned.

The training process used the Adam optimizer to update the network parameters by calculating the error between the predicted result and the true annotation according to the total loss function. The error was backpropagated to the deep neural network model, thereby calculating the gradient.

In this experiment, some 1.5T MRI data were collected from Beijing Sanbo Brain Hospital and Tsinghua Changgeng Hospital, and the 1.5T MRI image was super-resolved using the improved super-resolution model. Several examples of data sets are included in Table 2, and the information includes gender, age, number of layers, pixel side length, distance between layers, and magnetic field strength.

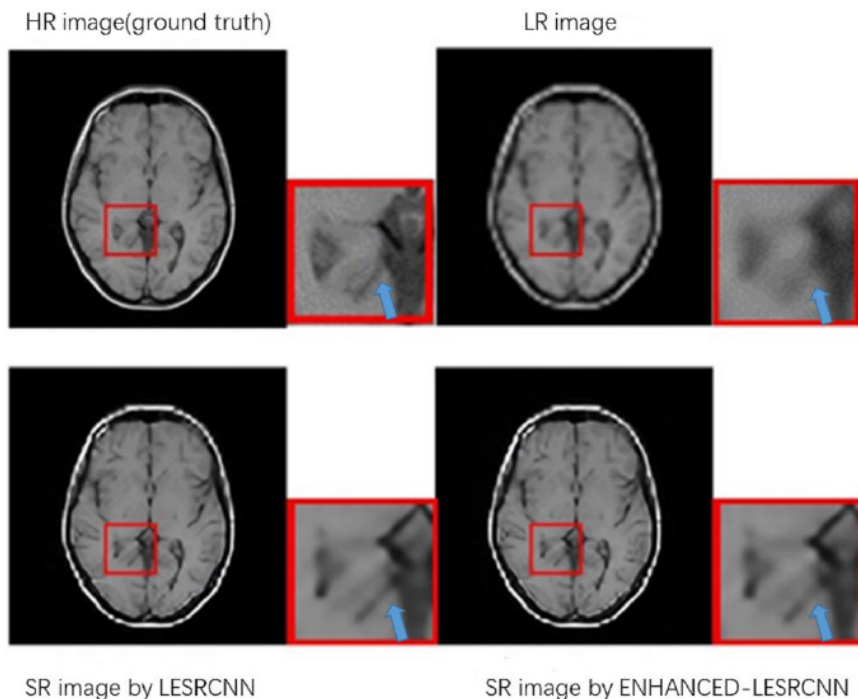
**Table 2. Samples of the dataset.**

No.	Gender	Age	Number of Layers	Pixel Side Length (mm)	Distance between Layers (mm)	Magnetic Field Strength (T)
235	F	30	22	0.2246	6.0	1.5
379	M	11	22	0.2246	6.0	1.5
401	F	16	22	0.2246	6.0	1.5
415	M	7	22	0.2246	6.0	1.5
518	F	37	22	0.2246	6.0	1.5

The experimental results of the Enhanced-LESRCNN were compared with the basic algorithm, such as SRGAN, SPSR, and LESRCNN. We selected PSNR, SSIM, PI, and LPIPS as the performance metrics. It can be observed from the comparison with the original version of LESRCNN that the new network structure provides more comprehensive information supervision for the learning of high-frequency features of the network due to the improvement in the global skip-connection, and PSNR and SSIM were found to be significantly better than those of the original network, demonstrating the effectiveness of the network structure of the global skip connection. The statistical results of the performance indicators are shown in Table 3. Some super-resolution samples and details are also shown in Fig. (3).

**Table 3.** Experiment result of our model.

<b>PSNR</b>	<b>0.5T</b>	<b>1.5T</b>
SRGAN	27.196	26.298
LESRCNN	28.836	28.419
SPSR	26.742	26.593
Enhanced LESRCNN	29.142	28.854
<b>SSIM</b>	<b>0.5T</b>	<b>1.5T</b>
SRGAN	0.681	0.743
LESRCNN	0.904	0.907
SPSR	0.659	0.814
Enhanced LESRCNN	0.910	0.915
<b>PI</b>	<b>0.5T</b>	<b>1.5T</b>
SRGAN	3.8505	4.0631
LESRCNN	5.7492	5.9175
SPSR	4.0948	3.8402
Enhanced LESRCNN	5.7623	5.9307
<b>LPIPS</b>	<b>0.5T</b>	<b>1.5T</b>
SRGAN	85.78%	82.99%
LESRCNN	86.73%	85.80%
SPSR	83.41%	82.39%
Enhanced LESRCNN	86.91%	86.20%

**Fig. (3).** Details of super-resolution samples.

In Fig. (3), the line segments pointed by the arrow in HR are relatively light-colored. The line segments obtained by Enhanced-LESRCNN are also light-colored and somewhat intermittent, which is closer to the line segments in HR and slightly different from the darker and more continuous line segments obtained by LESRCNN.

Due to the limited improvement, it is difficult to feel the

improved performance visually. We mainly demonstrated the effectiveness of our method through the indicators, as shown in Table 3.

Besides, the main purpose of our study is not to surpass all existing methods in algorithm performance but to emphasize that we can actually use them in clinical applications. Under the lack of computing resources and MRI scanners with high

field intensity in remote areas, rapid high-resolution reconstruction can be carried out. Therefore, obtaining the recognition of doctors is more important than algorithm performance indicators.

We fed back the results to five MRI doctors and collected subjective ratings from MRI doctors. They compared the results obtained by our algorithm with the original low-resolution figures and scored the clinical experience subjectively. We provided several options for the doctors to choose the range of improvement. The results are listed in Table 4. Three doctors believed that our recovery of details has improved by 5%-10%, and two doctors believed that it has improved by 3%-5%. On the whole, they concluded that there are some significant improvements in some details. Besides, they all agreed that our algorithm could be used clinically in remote areas and has great value. Getting the doctor's approval is the most important thing for our algorithm.

**Table 4. Doctor's evaluation results.**

Doctors	Improvement
Doctor1	5%-10%
Doctor2	3%-5%
Doctor3	3%-5%
Doctor4	5%-10%
Doctor5	5%-10%

At the same time, we recorded the model training speed after the model improvement and the original version, and after adding the network structure of the global skip connection, the running speed of the model was almost no more loss, indicating that if the super-resolution algorithm is applied to the clinic, our network structure improvement will make the model enhance performance without increasing the running cost of the model. The running time of models and the number of parameters of models are shown in Tables 5 and 6.

**Table 5. Running time of models.**

GPU(second/image)	0.5T	1.5T
LESRCNN	0.35	0.40
Enhanced-LESRCNN	0.36	0.42

**Table 6. Number of parameters of models.**

Model	Number of Parameters
LESRCNN	774040
Enhanced-LESRCNN	810904

The time complexity and space complexity are represented as follows:

$$\text{Time complexity} = O(\sum_{l=1}^D M_l^2 K_l^2 C_{l-1} C_l) \quad (8)$$

$$\text{Space complexity} = O(\sum_{l=1}^D K_l^2 C_{l-1} C_l + \sum_{l=1}^D M_l^2 C_l) \quad (9)$$

Where, O stands for the term reserved only for the highest degree, D represents the total number of convolution layers, l represents the current number of convolution layers,  $M_l$  represents the side length of feature map output by each

convolution kernel,  $K_l$  represents the side length of each convolution kernel size,  $C_l$  and  $C_{l-1}$  respectively, represent the number of output channels at layer l and (l-1).

Considering time complexity, according to the formula (8), given the same scale input, LESRCNN and Enhanced-LESRCNN had almost the same time complexity because most of the structures were the same, and skip connections caused little extra time complexity.

Regarding space complexity, according to the formula (9), the space complexity was determined by the space occupied by the total number of parameters and the output feature map of each layer. Given the same scale input, the space occupied by the feature maps of LESRCNN and Enhanced-LESRCNN was almost the same according to their structures. Besides, as shown in Table 6, the numbers of parameters of these two algorithms were close. Therefore, the space complexity of the two algorithms was almost the same.

The above results proved that the time complexity, space complexity, reasoning time, and numbers of parameters of Enhanced-LESRCNN and lightweight network LESRCNN were very close. Since LESRCNN is recognized as a lightweight model, Enhanced-LESRCNN is also a lightweight model, while SRGAN and SRSR methods lag far behind in SSIM and other indicators. Therefore, they were not compared in the time complexity, space complexity, and other issues of lightweight performance.

## CONCLUSION

In this study, considering the domain characteristic of MRI image data, a new network structure of global skip connection was proposed, maximizing the use of network feature learning from shallow to deep. We used transfer learning to train super-resolution networks, accelerating the training of deep network models on small-scale medical imaging data. In the experimental part, we used different magnetic field strength data and clinical data to verify the algorithm. The experimental results reported that the Enhanced-LESRCNN improved the objective indicators of the algorithm without significantly increasing running time. Our algorithm has realized the purpose of generating high-resolution MRI images in hospitals in remote areas lacking medical equipment by using MRI equipment with a low magnetic field and poor computing resources. As it is a lightweight network, it can operate in places where computing resources are scarce. The advantages mentioned above have been highly evaluated by doctors, who believe that it has important application value in clinical practice in remote areas.

## LIST OF ABBREVIATIONS

**MRI** = Magnetic Resonance Imaging

**IEEB** = Information Extraction and Enhancement

**RB** = Reconstruction Module

## ETHICS APPROVAL AND CONSENT TO PARTICIPATE

The collection and analysis of subjects' brain MRI images in this study were approved by the Ethics Committee of Beijing

Sanbo Brain Hospital and Tsinghua Changgeng Hospital.

## HUMAN AND ANIMAL RIGHTS

No humans or animals were used in the studies that are the basis of this research.

## CONSENT FOR PUBLICATION

Not applicable.

## AVAILABILITY OF DATA AND MATERIALS

We collected data from patients at Beijing Sanbo Brain Hospital and Tsinghua Changgeng Hospital. The raw data required to reproduce these findings cannot be shared currently as the data will be used in an ongoing study.

## FUNDING

This research was supported by the Foundation of Shenzhen Science and Technology Planning Project (NO.JCYJ20190809173411533 & GJHZ20200731095205015) and The Natural Science Foundation of Guangdong Province (No. 2022A1515011120).

## CONFLICT OF INTEREST

The authors declare no conflict of interest, financial or otherwise.

## ACKNOWLEDGEMENTS

The authors would like to thank Sanbo Brain Hospital and Tsinghua Changgeng Hospital for supporting this research.

## REFERENCES

- [1] Duchon CE. Lanczos filtering in one and two dimensions. *J Appl Meteorol* 1979; 18(8): 1016-22.  
[[http://dx.doi.org/10.1175/1520-0450\(1979\)018<1016:LFOAT>2.0.CO;2](http://dx.doi.org/10.1175/1520-0450(1979)018<1016:LFOAT>2.0.CO;2)]
- [2] Yang J, Wright J, Huang TS, et al. Image super-resolution as sparse representation of raw image patches. 2008 IEEE Computer Society Conference on Computer Vision and Pattern Recognition (CVPR 2008). 24-26 June 2008; Anchorage, Alaska, USA. IEEE. 2008.
- [3] Gao X. Image super-resolution with sparse neighbor embedding. *IEEE Transactions on Image Processing* 2012; 21(7): 3194.
- [4] Cvpr A, Id P. Convolutional sparse coding for image super-resolution. 2015 IEEE International Conference on Computer Vision (ICCV).
- [5] Dakua SP, Sahambi JS. Automatic left ventricular contour extraction from cardiac magnetic resonance images using cantilever beam and random walk approach. *Cardiovasc Eng* 2010; 10(1): 30-43.
- [6] [http://dx.doi.org/10.1007/s10558-009-9091-2] [PMID: 20082140]  
Dakua SP, Sahambi JS. Modified active contour model and Random Walk approach for left ventricular cardiac MR image segmentation. *Int J Numer Methods Biomed Eng* 2011; 27(9): 1350-61.  
[<http://dx.doi.org/10.1002/cnm.1430>]
- [7] Chao D, Chen CL, He K, et al. Learning a deep convolutional network for image super-resolution. European Conference on Computer Vision.
- [8] Kim J, Jung KL, Kyoung ML. Accurate image super-resolution using very deep convolutional networks. *arXiv:151104587* 2015.
- [9] Johnson J, Alahi A, Fei-Fei L. Perceptual Losses for Real-Time Style Transfer and Super-Resolution. Cham: Springer 2016.  
[[http://dx.doi.org/10.1007/978-3-319-46475-6\\_43](http://dx.doi.org/10.1007/978-3-319-46475-6_43)]
- [10] Ledig C, Theis L, Huszar F, et al. Photo-realistic single image super-resolution using a generative adversarial network. *arXiv:160904802* 2016.
- [11] Wang X, Yu K, Wu S, et al. ESRGAN: Enhanced super-resolution generative adversarial networks. > *arXiv:180900219* 2018.
- [12] Ma C, Rao Y, Cheng Y, et al. Structure-preserving super resolution with gradient guidance. 2020 IEEE/CVF Conference on Computer Vision and Pattern Recognition (CVPR).  
[<http://dx.doi.org/10.1109/CVPR42600.2020.00779>]
- [13] Caballero J. Cardiac image super-resolution with global correspondence using multi-atlas patchmatch. *Med Image Comput Comput Assist Interv* 2013; 16(Pt 3): 9-16.
- [14] Gao Y, Li H, Dong J, et al. A deep convolutional network for medical image super-resolution. 2017 Chinese Automation Congress (CAC).
- [15] Liu H, Xu J, Yan W, et al. Learning deconvolutional deep neural network for high resolution medical image reconstruction. *Inf Sci* 2018; 468: 142-54.
- [16] Ren S, Jain DK, Guo K, Xu T, Chi T. Towards efficient medical lesion image super-resolution based on deep residual networks. *Signal Process Image Commun* 2019; 75: 1-10.  
[<http://dx.doi.org/10.1016/j.image.2019.03.008>]
- [17] Bing X, Zhang W, Zheng L, Zhang Y. Medical image super resolution using improved generative adversarial networks. *IEEE Access* 2019; 7: 145030-8. [J].  
[<http://dx.doi.org/10.1109/ACCESS.2019.2944862>]
- [18] Agustsson E, Timofte R. NTIRE 2017 challenge on single image super-resolution: Dataset and study. 2017 IEEE Conference on Computer Vision and Pattern Recognition Workshops (CVPRW).
- [19] Zheng H, Qu X, Bai Z, et al. Multi-contrast brain magnetic resonance image super-resolution using the local weight similarity. *BMC Med Imaging* 2017; 17(1): 6.  
[<http://dx.doi.org/10.1186/s12880-016-0176-2>] [PMID: 28095792]
- [20] de Leeuw den Bouter ML, Ippolito G, O'Reilly TPA, Remis RF, van Gijzen MB, Webb AG. Deep learning-based single image super-resolution for low-field MR brain images. *Sci Rep* 2022; 12(1): 6362.  
[<http://dx.doi.org/10.1038/s41598-022-10298-6>] [PMID: 35430586]
- [21] Zhang R, Isola P, Efros AA, et al. The unreasonable effectiveness of deep features as a perceptual metric. 2018 IEEE/CVF Conference on Computer Vision and Pattern Recognition.  
[<http://dx.doi.org/10.1109/CVPR.2018.00068>]
- [22] Tian C, Zhuge R, Wu Z, et al. Lightweight image super-resolution with enhanced CNN [J]. *Knowledge-Based Systems* 2028; 205: 106235.  
[<http://dx.doi.org/10.1109/CVPR.2018.00068>]

